IEEE Access
Multidisciplinary ⋮ Rapid Review ⋮ Open Access Journal

Received 15 October 2023, accepted 24 November 2023, date of publication 30 November 2023,
date of current version 6 December 2023.

Digital Object Identifier 10.1109/ACCESS.2023.3337835

RESEARCH ARTICLE

An Inverse Kinematic Model for the 3-PRS Compliant Parallel Mechanism With Forward Causative Force

JUNJIE WEI, HAI BI, HONG YAO, AND FANGXIN CHEN, (Member, IEEE)
Jihua Laboratory, Foshan 528000, China

Corresponding author: Fangxin Chen (chenfx@jihualab.ac.cn)

This work was supported in part by the National Natural Science Foundation of China under Grant 52105020, in part by the Guangdong Basic and Applied Basic Research Foundation under Grant 2020B1515120068, in part by the National Key Research and Development Program of China under Grant 2021YFE0115700, and in part by the Youth Innovation Foundation of the Jihua Laboratory under Grant X220111XP220.

ABSTRACT The inverse kinematic model is an essential mathematical tool of the performance analysis and motion control for the parallel mechanism. A diversity of mathematical methods is used for inverse kinematic modelling. However, for compliant parallel mechanism, the direction of the causative force in the model is always disregarded in previous works, which leads to large deviation due to the force sensitivity of the flexure hinge. A straightforward index is proposed to quantitatively evaluate the deviation. A new approach presented in this paper try to overcome this shortcoming, by considering the forward causative force during the inverse kinematic modelling, which makes model realize less deviation and more practical in motion control. Compliant matrix method is adopted to analyze the deformation of the flexure hinge. The effectiveness of the proposed methodology is verified, based on a 3-PRS compliant parallel mechanism, with finite element analysis simulation. The proposed methodology can be employed and extended to a variety of compliant parallel mechanism.

INDEX TERMS Compliant mechanism, inverse kinetostatic model, compliant matrix method, 3-PRS.

I. INTRODUCTION

The compliant parallel mechanism (CPM) is a parallel mechanism whose joints are replaced by flexure hinges. In comparison to traditional parallel mechanisms, CPM realizes motion by elastic deformation of flexure parts, which by nature have no friction, backlash, or wear. Owing to these advantages, CPM has been widely employed in micro-electromechanical systems [1], precise positioning [2], micromanipulation [3], optical alignment [4], and other applications. Kinematic model is the basis of the motion control for the parallel mechanism. Generally, kinematic model can be divided into forward kinematic model (FKM) and inverse kinematic model (IKM). FKM can be defined as 'When the displacement of the active pair D_p given, solving the position and posture of the platform D_o', whereas IKM is defined as 'When the position and posture of the platform D_o is given, solving the displacement of the active pair D_p'. According to the definitions, FKM and IKM are reciprocal, which means that the solution of the FKM should be identical to the condition of the IKM, and vice verso.

In previous work, the rigid body inverse kinematic model (RIKM) is commonly used as an approximate IKM for the CPM, where the mechanical behavior of the flexure hinge is ignored and the geometric constraint of the kinematic chain is with ideal joints [5], [6], [7], [8]. RIKM provides a straightforward method for analyzing the kinematics of the CPM. However, since CPMs have an inherent coupling of kinematic-mechanical behaviors and complicated parallel arrangements, the kinematic behaviors differ from those of rigid-body equivalents. To improve the accuracy of the RIKM, some studies combined the force-displacement equations of the flexure hinge into the kinematic chain of the parallel mechanism [9], [10]. The flexure-based RIKM has

The associate editor coordinating the review of this manuscript and approving it for publication was Wonhee Kim.

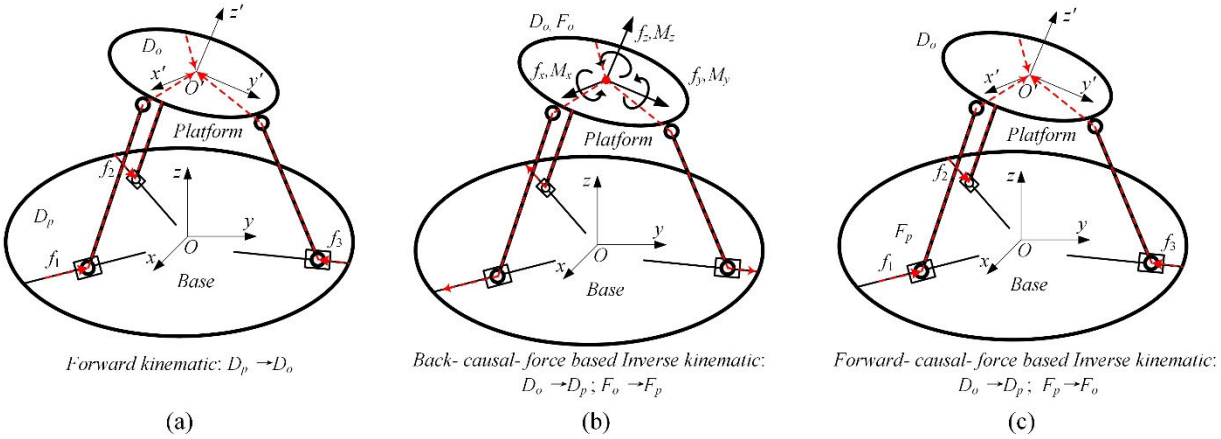

FIGURE 1. The illustrations of the FKM, BIKM, and FIKM.

a satisfactory accuracy. However, it is difficult to obtain analytical solution from the model due to the complexity of the equation set. Thus, the computation of the model is time-consuming. Castigliano's second theorem is an energy approach for analyzing the relationship between displacement and force in flexure hinges, which calculates the displacement of the flexible structure as the first-order differential of the total strain energy with respect to the corresponding external force. Yang et al. [10] developed the kinematic model of a six-DOF precision positioning stage using Castigliano's second theorem. The deviation between the FEA results and the generated model is approximate 20%. Author [11] was proposed a piezo-actuated microgripper for manipulation used. The Castigliano's second theorem and RIKM were utilized to analyze the motion performance of the microgripper, respectively. Lobontiu and Garcia [12] used the strain energy approach to develop an analytical model for displacement and stiffness of a bridge-type displacement amplifier. The predictions from the analytical model were within 5% of the FEA results. Although Castigliano's second theorem is concise, implementing inner-force analysis for CPM with complex configurations gets relatively challenging. This is why Castigliano's second theorem is a minority method for CPM modelling.

The reciprocity between the FKM and IKM is another issue in CMP's kinematics modeling, in addition to being time-consuming and complicated. Fig. 1(a) illustrates the FKM of the 3-PRS, with the causative forces running down the routes from the prismatic joints to the platform. Fig. 1 (b) shows the IKM, where the position and posture of the platform D_o is given and the causative forces are along the routes from the platform to the prismatic joints. Since the causative force is directed in the opposite direction as the FKM, the model shown in Fig. 1 (b) is called back-causative-force based inverse kinematic model (BIKM). Although the BIKM follows the definition of the IKM, the reverse causative force may cause a discrepancy between FKM and BIKM since the deformation of the flexure hinge is force sensitive. Fig. 1 (c) illustrates the forward causative force based inverse kinematic (FIKM), which is considered as a more practical IKM for CPM.

The compliant matrix approach is a kinetostatic modelling technique that does not include an inner-force analysis for the compliant mechanism [13], [14], [15]. However, some compliant matrix method based kinematic models for CPM are with back causative force assumption. Rouhani and Nategh [16] reported a kinetostatic solution to the IKM of a six-DOF CPM based on the compliant matrix of the flexure hinge. The screw theory was utilized to transfer the matrix. Xu et al. [17], [18] analyzed and designed two optoelectronic packaging used CPMs by using compliant matrix method. FEA and experimental study validate the accuracy of the established IKMs. Dan and Rui [9] presented an approach of the IKM of a six-DOF CPM with spatial beam flexure hinges. The model corresponds to the FEA results for the back causative force situation. The preceding efforts appear to have given a versatile answer to IKM of CPM. When the IKM solution is applied in forward kinematics simulation, however, a substantial deviation arises. Because the causative force does not correspond to the practical circumstance.

This paper presents an approach of the FIKM for a 3-PRS compliant parallel mechanism. The compliant matrix method is adopted to analyze the deformation of the flexure hinge. The prismatic joint is replaced by a flexure element with infinite flexibility to construct a close-loop kinematic chain. To quantify the deviation between the BIKM and FIKM, a new index, forward/inverse kinematic deviation rate (FIDR), is proposed. The finite element analysis (FEA) is used to validate the accuracy of the proposed FIKM. The results show that the FIDR between the FIKM and FEA are finer than the RIKM and BIKM. Furthermore, the proposed model provides an analytical solution, thus the computation time is short enough to be used in motion controlling.

The reminder of this paper is organized as follows. The FIDR of the rigid body 3-PRS and flexure-based one is exhibited in Section II. The compliance matrix based BIKM and FIKM are established in Section III. In Section IV,

the accuracy of the three models is validated by applying FEA. Finally, this paper is concluded in Section V.

II. THE DEVIATION BETWEEN FORWARD/INVERSE KINEMATICS

A. AN INDEX QUANTIFYING THE DEVIATION

When a target pose of the mechanism $\boldsymbol{D_o}$ is given, the required input displacements of the active joints $\boldsymbol{D_p}$ can be calculated by IKM. Then import the $\boldsymbol{D_p}$ into the controller to guide the parallel mechanism to reach the target pose $\boldsymbol{D'_o}$. Ideally, $\boldsymbol{D_o}$ and $\boldsymbol{D'_o}$ would be identical. In practice, deviation is exited due to machining error, assembly error, model error, and so forth. Previously mentioned index, FIDR, is used to quantify this deviation. The definition is formulated as follows:

$$\lambda_{FIDR}^{\bmod el1-\bmod el2} = \max\left(\frac{|d'_{O1}-d_{O1}|}{d'_{O1}} \ \frac{|d'_{O2}-d_{O2}|}{d'_{O2}} \ \cdots \ \frac{|d'_{On}-d_{On}|}{d'_{On}}\right) \quad (1)$$

where d_{oi} and d'_{oi} are the i^{th} element of vector $\boldsymbol{D_o}$ and $\boldsymbol{D'_o}$. The flow chart of the FIDR calculation is illustrated in Fig. 2.

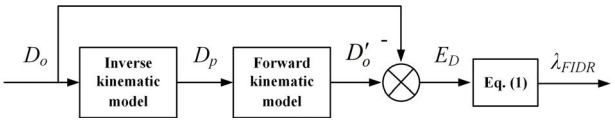

FIGURE 2. The flow chart of the FIDR.

B. RIGID BODY 3-PRS PARALLEL MECHANISM

Generally, a parallel mechanism is composed of a base, a platform, and multiple limbs. In the rigid body kinematics model, the joint is an idealization that does not consider any motion errors. Usually, solving the IKM needs to be based on the closed-loop kinematic chains implied in parallel mechanism, as shown in Fig. 3. In this case, the constraint equations of the closed-loop kinematic chain can be written as follows:

$$\overrightarrow{OO'}_{\{G\}} + R_{Euler} \cdot \overrightarrow{O'A_i}_{\{L\}} = \overrightarrow{OP_i}_{\{G\}} + s_i \cdot \frac{\overrightarrow{P_iB_i}_{\{G\}}}{\left|\overrightarrow{P_iB_i}_{\{G\}}\right|} + \overrightarrow{B_iA_i}_{\{G\}} \quad (2)$$

where the subscript $\{G\}$ indicates the vector is in the global coordinate system, $\{L\}$ indicates the vector is in the local coordinate system. R_{Euler} is the transformation matrix converted from Euler angle. It can be seen that the IKM result is the solving condition of the FKM issue in (34), and vice verso. Thus, the FIDR of rigid body kinematic model is zero.

C. THE 3-PRS COMPLIANT PARALLEL MECHANISM

In this part, the FIDR of the CPM is analyzed via finite element analysis (FEA) approach. The 3-D model of the 3-PRS was created by SolidWorks 2020, a commercial software for CAD. The model is then imported into Workbench, a commercial FEA simulation package. Fig. 4 shows the FEA model of the 3-PRS. The concerned structure parameters are set as variables that can auto-change according to the preestablished variable table. Threaded holes, fillets, and

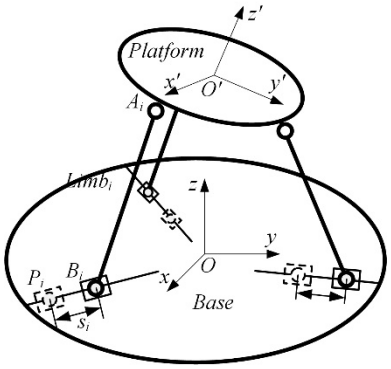

FIGURE 3. The illustration of the parallel mechanism.

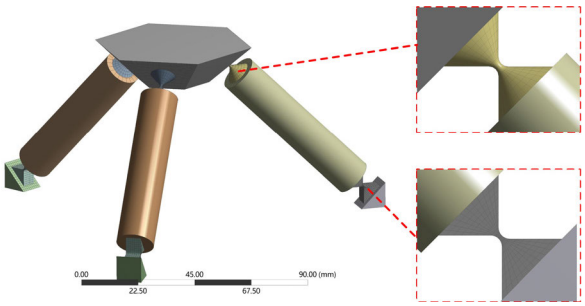

FIGURE 4. The FEA model of the 3-PRS in the co-simulation system.

other characteristics that have little effect on the FEA are deleted to reduce computing time. The flexure hinges that are the region of stress concentration are sliced for ease of meshing, with a mesh size of 0.2 mm. The revolute joint is made of spring steel with E-modulus of 210 GPa and Poisson's ratio of 0.3, while the ball joint is made of Aluminium alloy with E-modulus of 72 GPa and Poisson's ratio of 0.3. Table 1 lists the structure parameters.

TABLE 1. The structure parameters.

Geometry and properties	Symbol	Value	Unit
Length of the flexure hinge	l	5	mm
Width of the flexure higne	b	5	mm
Thickness of the flexure hinge	t	0.3	mm
Radius of the base	R_b	10	mm
Circumscribed circle radius of Platform	R_o	20	mm
Angle of kinematic chain	θ	45	°

Given the pose of the platform $\boldsymbol{D_o}$ set in Eq. (3), the displacements of the prismatic joints $\boldsymbol{D_p}$ is firstly obtained by FEA, and then set it to the corresponding prismatic joint of the kinematic chains to obtain a new pose of the platform $\boldsymbol{D'_o}$. The local coordinate system is set at the geometric center of the platform. The next procedures are followed the definition of the FIDR, as shown in Fig. 2.

$$\begin{aligned}
\mathbf{D_{o-\theta_x}} &= \left[\theta_x \ 0 \ 0\right], \ \text{with} \ \theta_x = 0:0.01:0.1(^\circ) \\
\mathbf{D_{o-\theta_y}} &= \left[0 \ \theta_y \ 0\right], \ \text{with} \ \theta_y = 0:0.01:0.1(^\circ) \\
\mathbf{D_{o-d_z}} &= \left[0 \ 0 \ d_z\right], \ \text{with} \ d_z = 0:0.01:0.1(mm)
\end{aligned} \quad (3)$$

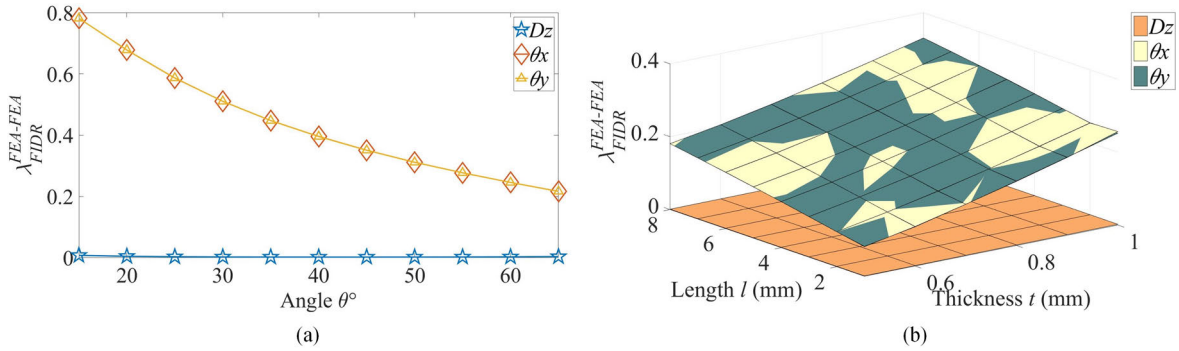

FIGURE 5. The result of the FIDR. (a) The structure angle θ *vs* λ_{FIDR}; (b) The flexure hinge parameters *vs* λ_{FIDR}.

The deviation of the FIDR is caused by the flexure hinge. Thus, the relations of the λ_{FIDR} with the flexure hinge parameters and the angle θ is analyzed. Fig. 5 shows the analysis results. When the platform moves along Z axis, λ_{FIDR} remains small. It is because that the motions of the three kinematic chains are centrosymmetric. Thus, the motion deviations caused by the flexure hinge is counteracted. The other two motions, i.e., rotations about X axis and Y axis, have extremely large λ_{FIDR}. Particularly, λ_{FIDR} increases while angle θ decreases and the length of flexure hinge l increases. The thickness t has little influence on the FIDR. The results reveal that the inverse kinematic model and the forward given of the flexure-based 3-PRS have large deviation, which is totally different from the rigid model expressed by Eq. (34). Thus, the IKM of the CMP should be reconsidered.

III. THE BIKM AND FIKM OF THE 3-PRS CPM

A. COMPLIANT MATRIX OF THE FLEXURE HINGE

Fig. 6 illustrates a flexure hinge with one end fixed and another free. When a force system $\boldsymbol{F}$ is applied at the free end, the displacement $\boldsymbol{D}$ can be calculated as follows:

$$\boldsymbol{D}_{\{h\}} = \boldsymbol{C}^h \cdot \boldsymbol{F}_{\{h\}} \tag{4}$$

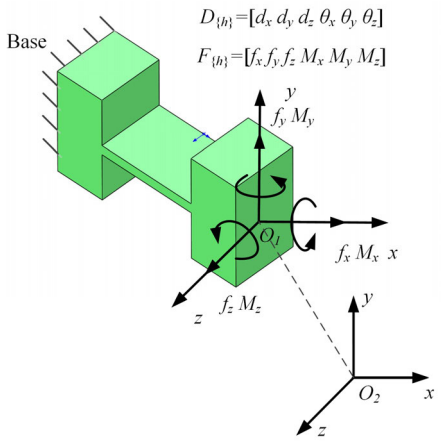

FIGURE 6. The flexure hinge and the coordinate system.

where subscript h indicates that the matrix or vector are expressed in flexure hinge fixed local coordinate system. $\boldsymbol{C}^h$ is the compliant matrix of the flexure hinge. In the global coordinate system, the transferred force and displacement from point a to point b can be obtained by matrix transformation

$$\begin{cases} \boldsymbol{D}_{a\{G\}} = \underbrace{[\boldsymbol{T}_{b-a}]^T \left[\boldsymbol{R}_{\{h\}-\{G\}}\right]^T}_{\boldsymbol{J}^D_{G-h}} \boldsymbol{D}_{b\{h\}} \\ \boldsymbol{F}_{b\{h\}} = \underbrace{\left[\boldsymbol{R}_{\{h\}-\{G\}}\right][\boldsymbol{T}_{b-a}]}_{\boldsymbol{J}^F_{h-G}} \boldsymbol{F}_{a\{G\}} \end{cases} \tag{5}$$

Substituting Eq. (5) into Eq. (4),

$$\boldsymbol{D}_{a\{G\}} = [\boldsymbol{T}_{h-a}]^T \left[\boldsymbol{R}_{\{h\}-\{G\}}\right]^T \boldsymbol{C}^h \left[\boldsymbol{R}_{\{h\}-\{G\}}\right][\boldsymbol{T}_{h-a}]\boldsymbol{F}_{a\{G\}} \tag{6}$$

For conciseness, two operators are utilized to replace Eq. (5) and Eq. (6).

$$\begin{aligned} Eq.(5): & \begin{cases} \boldsymbol{D}_{\{G\}} = \boldsymbol{J}^D_{G-h}\boldsymbol{D}_{\{h\}} \\ \boldsymbol{F}_{\{h\}} = \boldsymbol{J}^F_{h-G}\boldsymbol{F}_{\{G\}} \end{cases} \\ Eq.(6): & \boldsymbol{D}_{\{G\}} = \left(\boldsymbol{J}_{G-h} \otimes \boldsymbol{C}^h\right) \cdot \boldsymbol{F}_{\{G\}} \end{aligned} \tag{7}$$

The detailed calculation process of $\boldsymbol{C}^h$ can be referred to Appendix B1.1, while $\boldsymbol{T}$ and $\boldsymbol{R}$ can be referred to Appendix B1.2.

B. THE BIKM OF THE 3-PRS

According to the definition of the IKM, the pose of the CPM $\boldsymbol{D_o}$ is given, as shown in Fig. 1(b). Isolate i^{th} kinematic chain as a free-body. The force system that causes the kinematic chain deforming is $\boldsymbol{F_{oi}}$. Ignoring the nonlinear behavior, the displacement and the force at the free end of the kinematic chain can be expressed as follows:

$$\boldsymbol{D}_{oi-F_{oi}} = \boldsymbol{C}^{limbi}_{o-F_{oi}} \cdot \boldsymbol{F}_{oi} \tag{8}$$

while $\boldsymbol{D}_{oi-F_{oi}}$ can be calculated in another form:

$$\boldsymbol{D}_{oi-F_{oi}} = \boldsymbol{J}^D_{oi-o}\boldsymbol{D}_o = \boldsymbol{D}_o \tag{9}$$

$\boldsymbol{J}^{D}_{oi-o}$ is always identity matrix, since point oi and point o are coincident.

Where $\boldsymbol{C}^{limbi}_{o-F_{oi}}$ is the compliant matrix of i^{th} kinematic chain, which can be obtained by summing up the flexure elements in the kinematic chain:

$$\boldsymbol{C}^{limbi}_{o-F_{oi}} = \boldsymbol{J}_{o-pi} \otimes \boldsymbol{C}^{pi} + \boldsymbol{J}_{o-h1} \otimes \boldsymbol{C}^{h1} + \boldsymbol{J}_{o-h2} \otimes \boldsymbol{C}^{h2} \tag{10}$$

According to Eq. (5), the equivalent force of $\boldsymbol{F_{oi}}$ to respect to the input end can be written as follows:

$$\boldsymbol{F}_{pi} = \boldsymbol{J}^{F}_{pi-o}\boldsymbol{F}_{oi} \tag{11}$$

Substituting Eq. (11) into Eq. (8),

$$\boldsymbol{F}_{pi} = \boldsymbol{J}^{F}_{pi-o} \cdot \left[\boldsymbol{C}^{limbi}_{o-F_{oi}}\right]^{-1} \boldsymbol{D}_{o-F_{oi}} \tag{12}$$

Substituting Eq. (12) and Eq. (9) into Eq. (4),

$$\boldsymbol{D}_{pi} = \boldsymbol{C}^{pi} \cdot \boldsymbol{J}^{F}_{pi-o} \cdot \left[\boldsymbol{C}^{limbi}_{o-F_{oi}}\right]^{-1} \cdot \boldsymbol{D}_{o} \tag{13}$$

The whole kinematic chain of 3-PRS can be written as follows:

$$\boldsymbol{D}_{p} = [\boldsymbol{D}_{p1}\ \boldsymbol{D}_{p2}\ \boldsymbol{D}_{p3}\ ] = {}^{back}\boldsymbol{C}_{p-o} \cdot \boldsymbol{D}_{o} \tag{14}$$

with

$$\begin{aligned} {}^{back}\boldsymbol{C}_{p-o} &= \left[{}^{back}\boldsymbol{C}_{p1-o}\ {}^{back}\boldsymbol{C}_{p2-o}\ {}^{back}\boldsymbol{C}_{p3-o}\right] \\ {}^{back}\boldsymbol{C}_{pi-o} &= \boldsymbol{C}^{pi} \cdot \boldsymbol{J}^{F}_{pi-o} \cdot \left[\boldsymbol{C}^{limbi}_{o-F_{oi}}\right]^{-1} \end{aligned} \tag{15}$$

Eq. (14) describes the relation of the platform pose $\boldsymbol{D_O}$ and the input displacement $\boldsymbol{D_p}$. It follows the definition of the IKM. This modelling approach are widely used for CPM analysis [16], [17], [18], [19]. However, Eq. (11) shows the causative force is at the output end. It does not match with the case in the forward kinematics. Thus, this model is called back-causative-force based kinetostatic model.

C. THE FIKM OF THE 3-PRS

In forward-causative-force case, assume that $\boldsymbol{F_{pi}}$ is the causative force at the prismatic joint. The displacement at output end of the fictitious limb caused by $\boldsymbol{F_{pi}}$ can be expressed as follows, and the definition of fictitious limb can be found in Appendix B1.4.:

$$\boldsymbol{D}_{o-F_{pi}} = \boldsymbol{C}^{flimbi}_{o-F_{pi}} \cdot \boldsymbol{F}_{pi} \tag{16}$$

with

$$\boldsymbol{C}^{flimbi}_{o-F_{pi}} = \boldsymbol{J}^{D}_{o-pi}\boldsymbol{C}_{pi} \tag{17}$$

On the other hand, assume a virtual force $\boldsymbol{F}^{virtual}_{o}$ applied at the end of fictitious limb the displacement at the output end can be expressed as follows:

$$\mathbf{D}_{o-F_o} = \mathbf{C}^{flimbi}_{o-Fo} \cdot \mathbf{F}^{virtual}_{o} \tag{18}$$

Suppose that these two cases lead to a totally same displacement, i.e., $D_{o-Fpi} = D_{o-Fo}$. The virtual force $\boldsymbol{F}^{virtual}_{o}$ can be calculated as follows,

$$\mathbf{F}^{virtual}_{o} = [\mathbf{C}^{flimbi}_{o-Fo}]^{-1} \cdot \mathbf{C}^{flimbi}_{o-F_{pi}} \cdot \mathbf{F}_{pi} \tag{19}$$

Refer to Appendix B1.3, a 3-PRS can be consider as a parallel connection of springs, whose compliance matrix can be obtained by using the rule of equivalent stiffness:

$$\boldsymbol{D}_{o-Fo} = \boldsymbol{C}^{CPM}_{o-F_o} \cdot \boldsymbol{F}_{o} \tag{20}$$

with

$$\boldsymbol{C}^{CPM}_{o-F_o} = \left(\left[\boldsymbol{C}^{flimb1}_{o-F_o}\right]^{-1} + \left[\boldsymbol{C}^{flimb2}_{o-F_o}\right]^{-1} + \left[\boldsymbol{C}^{flimb3}_{o-F_o}\right]^{-1}\right)^{-1} \tag{21}$$

Substituting Eq. (19) to Eq. (52), displacement on point O caused by the input force is obtained:

$$\mathbf{D}_{o-F_{pi}} = \mathbf{C}^{CPM}_{o-F_o} \cdot [\mathbf{C}^{flimbi}_{o-Fo}]^{-1} \cdot \mathbf{C}^{flimbi}_{o-F_{pi}} \cdot \mathbf{F}_{pi} \tag{22}$$

The relationship between the input force of the three limbs and the displacement of the moving platform can be further expressed in the form of a matrix:

$$\boldsymbol{D}_{o-F_p} = \boldsymbol{C}^{CPM}_{o-F_p} \cdot \boldsymbol{F}_{p} \tag{23}$$

with

$$\begin{aligned} \boldsymbol{F}_{p} &= [\,F_{p1}\ F_{p2}\ F_{p3}\,] \\ \boldsymbol{C}^{CPM}_{o-F_p} &= \left[\boldsymbol{C}^{CPM}_{o-F_{p1}}\ \boldsymbol{C}^{CPM}_{o-F_{p2}}\ \boldsymbol{C}^{CPM}_{o-F_{p3}}\right] \\ \boldsymbol{C}^{CPM}_{o-F_{pi}} &= \boldsymbol{C}^{CPM}_{o-F_o} \cdot \left[\boldsymbol{C}^{flimbi}_{o-F_o}\right]^{-1} \cdot \boldsymbol{C}^{flimbi}_{o-F_{pi}} \end{aligned} \tag{24}$$

The displacement of the prismatic joint can be expressed as follows:

$$\boldsymbol{D}_{p-F_p} = \boldsymbol{C}^{CPM}_{p-F_p} \cdot \boldsymbol{F}_{p} \tag{25}$$

with

$$\begin{aligned} \boldsymbol{C}^{CPM}_{p-F_p} &= \left[\boldsymbol{C}^{CPM}_{p1-F_{p1}}\ \boldsymbol{C}^{CPM}_{p2-F_{p2}}\ \boldsymbol{C}^{CPM}_{p3-F_{p3}}\right] \\ \boldsymbol{C}^{CPM}_{pi-F_{pi}} &= \boldsymbol{C}^{CPM}_{p-F_o} \cdot \left[\boldsymbol{C}^{flimbi}_{o-Fo}\right]^{-1} \cdot \boldsymbol{C}^{flimbi}_{o-F_{pi}} \end{aligned} \tag{26}$$

where $\boldsymbol{C}^{CPM}_{p-F_o}$ is the transpose of $\boldsymbol{C}^{CPM}_{o-F_p}$,

$$\boldsymbol{C}^{CPM}_{p-F_o} = \left[\boldsymbol{C}^{CPM}_{o-F_p}\right]^{T} \tag{27}$$

Combined Eq. (23) and Eq. (25), the FIKM can be expressed as follows:

$$\boldsymbol{D}_{p-F_p} = \boldsymbol{C}^{CPM}_{p-F_p} \cdot \left[\boldsymbol{C}^{CPM}_{o-F_p}\right]^{\dagger} \cdot \boldsymbol{D}_{o-F_p} \tag{28}$$

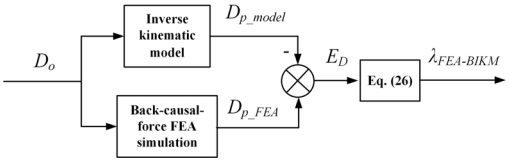

FIGURE 7. The flow chart of the accuracy validation of the model.

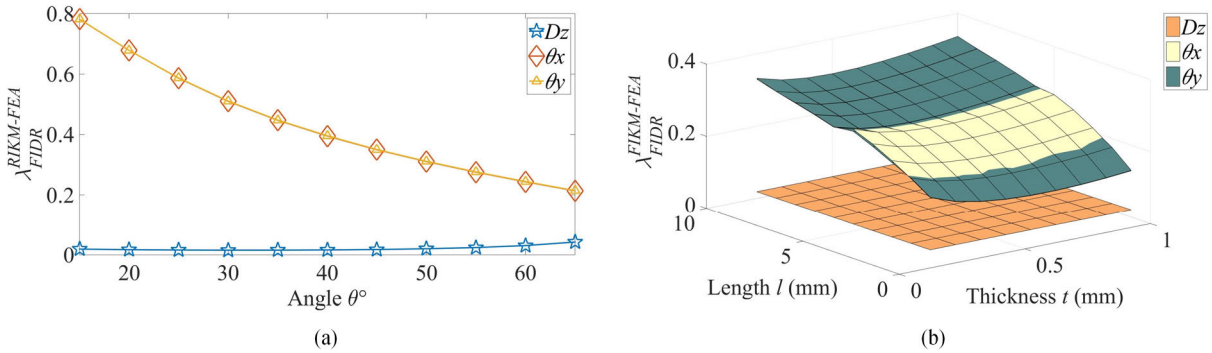

FIGURE 8. The FIDR of RIKM – FEA: (a) $\lambda_{FIDR}^{RIKM-FEA}$ *vs* angle θ; (b) $\lambda_{FIDR}^{RIKM-FEA}$ *vs* flexure hinge parameters.

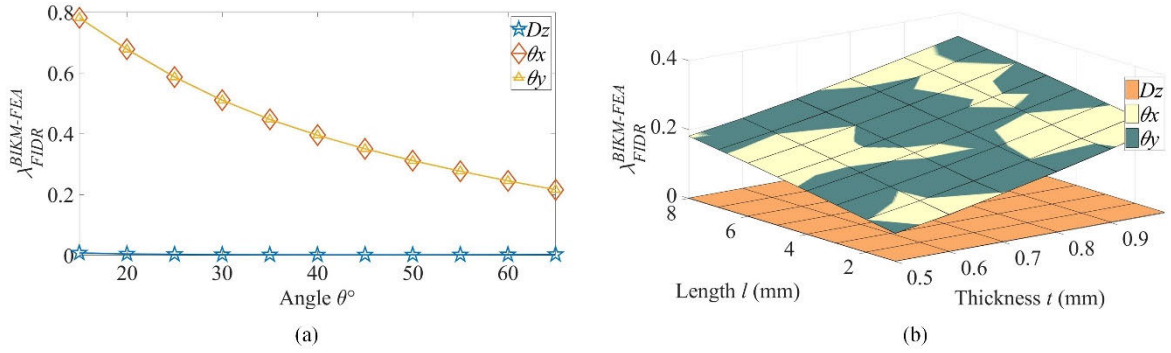

FIGURE 9. The FIDR of BIKM – FEA: (a) $\lambda_{FIDR}^{BIKM-FEA}$ *vs* angle θ; (b) $\lambda_{FIDR}^{BIKM-FEA}$ *vs* flexure hinge parameters.

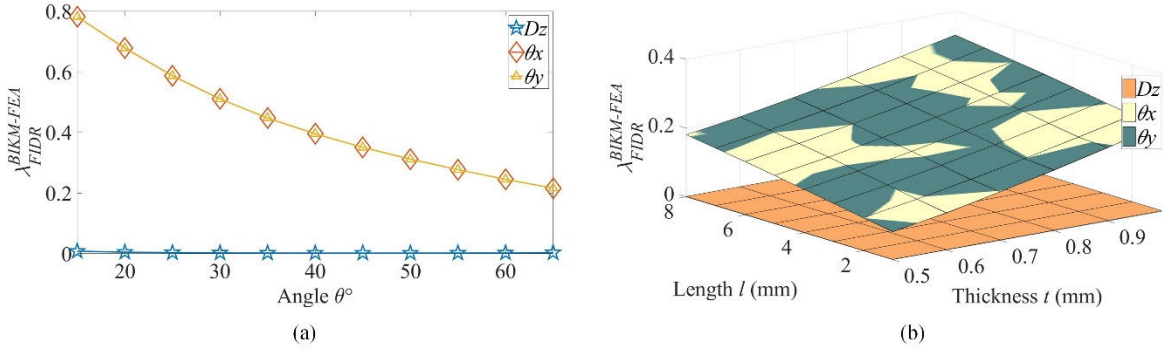

FIGURE 10. The FIDR of BIKM – FEA: (a) $\lambda_{FIDR}^{BIKM-FEA}$ *vs* angle θ; (b) $\lambda_{FIDR}^{BIKM-FEA}$ *vs* flexure hinge parameters.

IV. FEA VALIDATION

In order to verify the established model, the predictions are compared to the FEA results. The compliant matrix of the V-shape flexure hinge can be found in [20]. The structure parameters of the of the model are listed in Table 1.

A. ACCURACY OF THE BIKM

To quantify the accuracy of the BIKM, the deviation ratio is defined as follows:

$$\zeta^{FEA-BIKM} = \max\left(\frac{|d_{EFA1}-d_{BIKM1}|}{d_{EFA1}} \quad \frac{|d_{EFA2}-d_{BIKM2}|}{d_{EFA2}} \quad \frac{|d_{EFA3}-d_{BIKM3}|}{d_{EFAn}}\right) \quad (29)$$

where $\boldsymbol{d_{EFAi}}$ and $\boldsymbol{d_{BIKMi}}$ are the i^{th} element of the displacement vector solved from the FEA and theoretic model, respectively. Fig. 7 illustrates the flow chart of the accuracy validation.

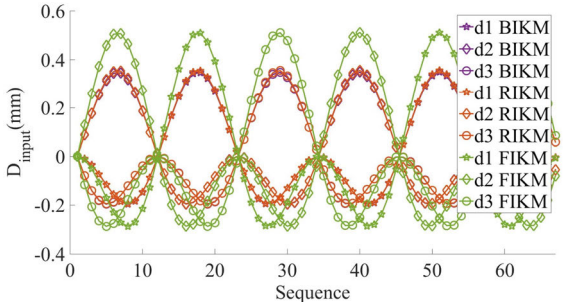

FIGURE 11. The input displacement sequence of the trefoil.

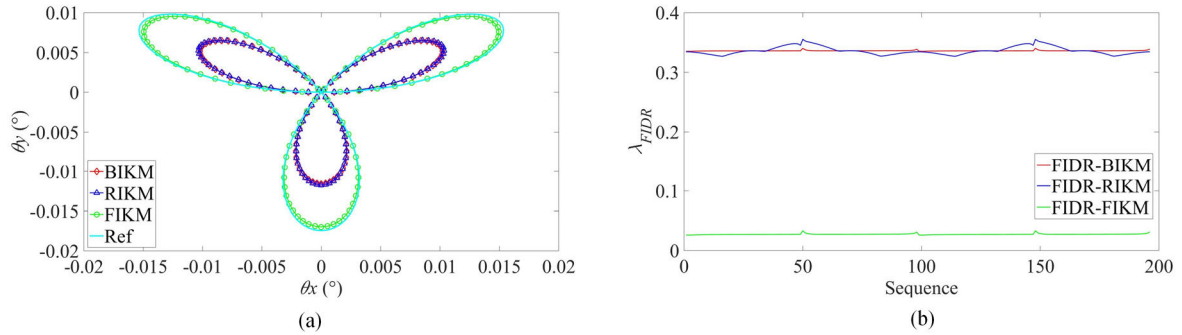

FIGURE 12. The trefoil trajectory of the 3-PRS: (a) The D_o of the trefoil trajectory; (b) The λ_{FIDR} of the three models.

The FEA results in Section II are reused. The BIKM established in Section III is utilized to calculate the theoretic predictions, where the structure and material parameters are consistent with the FEA simulation. The number of the samples is 180. Each sample date is processed by Eq. (28). Table 2 lists the statistical result of the deviation ratio. The maximum error is 3.31%, the minimum one is 0.12%, the mean is 1.81%, and the median is 1.46%. The results show that the BIKM has an extremely high accuracy for back causative force-based motion.

TABLE 2. The statistical result of the deviation ratio.

Samples	Max	Min	Mean	median
180	3.31%	0.12%	1.81%	1.46%

B. THE FIDR OF THE RIKM, BIKM AND FIKM

Although the BIKM has a great consistency and accuracy compared with FEA results, it is not appropriate to be used in motion control due to the force status is inconsistent with the forward case. The FIDR is a straightforward index to assess the theoretical model that can be used for motion control or not. In this part, the FIDR of the RIKM, BIKM and FIKM with the FEA are presented, respectively. First, give the expected poses of the platform $\mathrm{D_O^{expected}}$, which is listed in Eq. (3). Second, use the RIKM, BIKM and FIKM to calculate the displacement at prismatic joint $\mathrm{D_p^{RIKM}D_p^{BIKM}}$ and $\mathrm{D_p^{FIKM}}$, respectively. Then, import $\mathrm{D_p^{RIKM}D_p^{BIKM}}$ and $\mathrm{D_p^{FIKM}}$ to the FEA software and obtain the pose of the platform $\mathrm{D_O^{RIKM-FEA}}$, $\mathrm{D_O^{BIKM-FEA}}$ and $\mathrm{D_O^{FIKM-FEA}}$, respectively. Finally, calculate the FIDR by Eq. (3).

Fig. 8 shows the analysis results of the RIKM. No matter how angle θ and flexure hinge parameters change, $\lambda_{FIDR}^{RIKM-FEA}$ remains small when the platform moves along Z axis due to the symmetric distribution of the force. As for the other two DOFs, the $\lambda_{FIDR}^{RIKM-FEA}$ is large. Particularly, $\lambda_{FIDR}^{RIKM-FEA}$ increases with angle θ reduce and length l increase.

Fig. 9 is the analysis results of the BIKM. The relation of the $\lambda_{FIDR}^{BIKM-FEA}$ with the variables are almost identical with the FEA-FEA result shown in Fig. 5. It is because that the input displacement calculated by BIKM and obtained by FEA are closed, as shown in Table 2.

Fig. 10 presents the results of the FIKM. The deviation is significant reduced compared with the other two IKMs. Specifically, $\lambda_{FIDR}^{RIKM-FEA}$ increase with angle θ decrease. the maximum deviation value is within 0.1. As for the flexure hinge parameters, short l and large t bring small $\lambda_{FIDR}^{RIKM-FEA}$. The largest deviation is within 0.13.

Overall, the three IKM models are able to provide fine prediction when the platform moves along Z axis. However, for the other two DOFs, RIKM and BIKM have a large deviation of FIDR, which is sensitive to angle θ and flexure hinge parameters. On the contrary, FIKM keeps a fine prediction on the other two DOFs. The maximum deviation is within 13%. Thus, FIKM is an IKM accurate enough to be used in structure design and kinematics control.

C. THE COMPOUND MOTION OF THE 3-PRS

According to the analysis results shown in Fig. 8 -Fig. 10, the two rotation DOFs has a large deviation of the FIDR. Thus, it is necessary to test the compound motions containing rotation around X and Y axes. To do so, a trefoil trajectory is used, which can be expressed as follows:

$$D_o = \begin{bmatrix} \theta_x & \theta_y & 0 \end{bmatrix} \tag{30}$$

with

$$\begin{cases} \theta_x = \sin(3t) \cdot \cos(t) \\ \theta_y = \cos(3t) \cdot \sin(t) \end{cases} \tag{31}$$

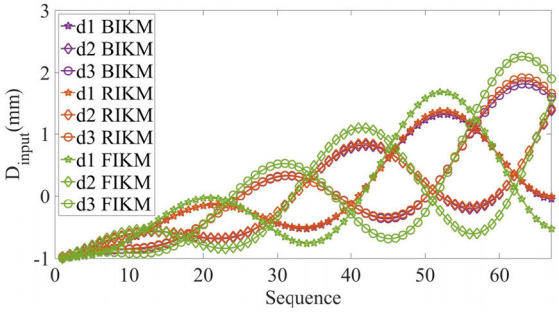

FIGURE 13. The input displacement sequence of the helix.

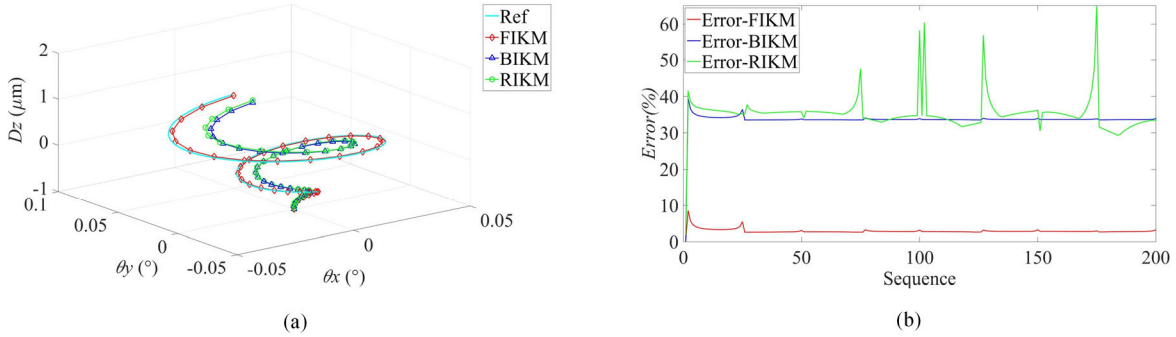

FIGURE 14. The helix line trajectory of the 3-PRS: (a) The D_o of the helix trajectory; (b) The λ_{FIDR} of the three models.

Calculate the input displacements by RIKM, BIKM, and FIKM respectively. Fig. 11 illustrates the calculation results. Then, import the input vectors D_p^{RIKM}, D_p^{BIKM} and D_p^{FIKM} into the FEA model and obtain the pose of the platform $D_O^{RIKM-FEA}$, $D_O^{BIKM-FEA}$ and $D_O^{FIKM-FEA}$, respectively.

Fig. 12 presents the results of the trefoil trajectory of the 3-PRS. The trajectory of the FIKM is much close to the reference one with deviations within 0.03. On the contrary, the RIKM and BIKM are far away from the reference trajectory with deviations larger than 0.35. It implies that the proposed FIKM is able to predict the compound motions with two rotations.

It is known that the 3-PRS has three motion DOFs including θ_x, θ_y, d_z. A spatial trajectory, helix line, is utilized to test, which can be formulated as follows:

$$\begin{cases} \theta_x = \dfrac{t}{240} \cdot \sin(t) \\ \theta_y = \dfrac{t}{240} \cdot \cos(t) \\ d_z = \dfrac{(t - 2\pi) \times 10^{-3}}{2\pi} \end{cases} \tag{32}$$

The input displacements of the prismatic joints obtained by IKM models are illustrated in Fig. 13. The analysis results are presented in Fig. 14, which shows that the FIKM has the finest prediction with a deviation within 0.08. The other two IKM models performs bad with deviations larger than 0.4.

V. CONCLUSION

This paper discussed the inverse kinematic modelling of the flexure-based 3-PRS parallel mechanism. The deviation between the BIKM and FKM of the CPM was exhibited via FEA simulation. To quantify the deviation, a new index, FIDR, was proposed. FEA studies showed that the deviation of the flexure-based 3-PRS is larger than 0.8, which is sensitive to angle θ and flexure hinge parameters. three IKM models are established to predict the motion of the 3-PRS. RIKM has a large deviation due to the neglect of the flexure hinge. BIKM is unsatisfying since the causative force in the model is opposite to the practical situation. Final, the improved model, FIKM, provides a great prediction on the complex compound trajectory with a maximum deviation within 8% that is fine enough to be used on kinematic control. The simulation results validate the effectiveness of the proposed methodology that can be employed and extended to a variety of compliant parallel mechanism.

APPENDIX A

See Table 3.

APPENDIX B

A. DERIVATION OF THE COMPLIANCE MATRIX OF FLEXURE HINGE

Compliance matrix describes the force-deformation relationship of a flexure hinge, it can be derived according to Castigliano's theorem. Since the flexure hinges used in this paper have V-shaped in front view, takes the V-shaped revolute joint and V-shaped spherical joint as example, the derivation of their compliance matrix can be carried out by the following steps:

a) Formulate the function of the V-shape:

$$y(x) = \begin{cases} l/2 + t/2 + (1 - \sqrt{2})r - x, \\ \qquad x \in [0, l/2 - \sqrt{2}/2r] \\ t/2 + r - \sqrt{r^2 - (x - l/2)^2}, \\ \qquad x \in [l/2 - \sqrt{2}/2r, l/2 + \sqrt{2}/2r] \\ -l/2 + t/2 + (1 - \sqrt{2})r + x, \\ \qquad x \in [l/2 + \sqrt{2}/2r, l] \end{cases} \tag{33}$$

b) Assuming the force $F = [f_x\ f_y\ f_z\ M_x\ M_y\ M_z]^T$ acted on the free end of the flexure hinge and deform it, according to the Clapeyron theorem, the elastic strain energy equals to the work of F, it can be formulated as follows:

$$V = \int_0^l \frac{F_x(x)^2}{2EA}dx + \int_0^l \frac{\alpha F_y(x)^2}{2GA}dx + \int_0^l \frac{\alpha F_z(x)^2}{2GA}dx + \int_0^l \frac{M_x(x)^2}{2GI_p}dx + \int_0^l \frac{M_y(x)^2}{2EI_y}dx + \int_0^l \frac{M_z(x)^2}{2EI_z}dx \tag{34}$$

where α is shear coefficient, I_y and I_z is moment of inertia about y axis and z axis, I_p is polar moment of inertia, A is cross

TABLE 3. Nomenclature

Symbol	Quantity
pi	i^{th} Prismatic joint.
o	Center point of moving platform.
oi	End point of i^{th} limb. In fact, oi and o are coincident.
$\{h\}$	Coordinate system fixed on the free end of flexure hinge.
$\{G\}$	Global coordinate system.
θ	Angle between limb and base at initial configuration.
h	Origin of coordinate system $\{h\}$.
r_{top}	Circumscribed circle radius of Platform.
$\boldsymbol{D}_{\{h\}}$	Displacement vector with dimension 6×1 , expressed in {h} coordinate, composed in the following order: $\begin{bmatrix} d_x & d_y & d_z & \theta_x & \theta_y & \theta_z \end{bmatrix}^T$.
$\boldsymbol{D}_{o-F_{oi}}$	Displacement vector at point o, caused by the force acted on point oi
$\boldsymbol{F}_{\{h\}}$	Force vector with dimension 6×1 , expressed in {h} coordinate, composed in the following order: $\begin{bmatrix} f_x & f_y & f_z & M_x & M_y & M_z \end{bmatrix}^T$.
$\boldsymbol{C}^h$	Compliance matrix of flexure hinge, with dimension 6×6 .
$\boldsymbol{C}^{limbi}_{o-F_{oi}}$	Compliance matrix of i^{th} limb , represent the relationship between force(acted on point oi) and displacement (at point o).
$\boldsymbol{C}^{CPM}_{p-F_p}$	Compliance matrix of CPM, represent the relationship between force(acted on prismatic joint) and displacement (at prismatic joint p).
$\boldsymbol{C}^{CPM}_{o-F_o}$	Compliance matrix of CPM, represent the relationship between force(acted on point o) and displacement (at point o).
$\boldsymbol{T}_{h-G}$	Transformation matrix with dimension 6×6 , convert a force acting on point G into a equivalent force acting on point h
$\boldsymbol{R}_{\{h\}-\{G\}}$	Rotation matrix, also called directional cosine matrix, with dimension 6×6 . It is used to transform a vector in a {G} coordinate system into {h} coordinate system.
$\boldsymbol{J}^D_{G-h}$	Displacement equivalent matrix with dimension 6×6 .
$\boldsymbol{J}^F_{h-G}$	Force equivalent matrix with dimension 6×6 .
$\boldsymbol{J}_{G-h}$	Equivalent matrix with dimension 6×6 .

sectional area. All of them are geometric related parameters, i.e., can be calculated by $y(x)$ [5], [21], [22]. G and E is shear modulus and elastic modulus, respectively.

$$\begin{cases} F_x(x) = f_x \\ F_y(x) = f_y \\ F_z(x) = f_z \\ M_x(x) = M_x \\ M_y(x) = f_z x + M_y \\ M_z(x) = -f_y x + M_z \end{cases} \tag{35}$$

c) The relationship between the deformation vector and the load vector can be expressed as follows:

$$\Delta = \frac{\partial V}{\partial F_i} = C_{ij} \cdot F_j \tag{36}$$

where F_i means the i^{th} element of F, and C_{ij} is the element of compliance matrix at (i, j).

Now, complete compliance matrix is obtained by (4).

B. DERIVATION OF THE TRANSFORMATION MATRIX AND ROTATION MATRIX

1) ROTATION MATRIX $R_{\{A\}-\{B\}}$

Suppose that frame B could be convert by frame A though a series rotation about z-y-x axis in sequence with respective angle γ, β, α, then the rotation matrix is formulated as:

$$\begin{aligned} {}^{A\rightarrow B}_{\quad}\boldsymbol{Q}\,(\alpha,\beta,\gamma) = &\begin{bmatrix} 1 & 0 & 0 \\ 0 & c\alpha & -s\alpha \\ 0 & s\alpha & c\alpha \end{bmatrix} \begin{bmatrix} c\beta & 0 & s\beta \\ 0 & 1 & 0 \\ -s\beta & 0 & c\beta \end{bmatrix} \\ &\times \begin{bmatrix} \mathbf{c}\gamma & -s\gamma & 0 \\ s\gamma & c\gamma & 0 \\ 0 & 0 & 1 \end{bmatrix} \end{aligned} \tag{37}$$

A three-dimension vector in frame B can be expressed in frame A by following transformation:

$$v_{\{A\}} = {}^{A\rightarrow B}_{\quad}\boldsymbol{Q} \cdot v_{\{B\}} \tag{38}$$

In this paper, since no matter force vector or deformation vector are six-dimension, and the first three-dimensional and the last three-dimensional represent the quantities along/about the three coordinate axes respectively, the rotation matrix is furtherly formulates as:

$$R_{\{A\}-\{B\}}(\alpha,\beta,\gamma)=\begin{bmatrix} {}^{A\to B}_{\quad}Q & 0 \\ 0 & {}^{A\to B}_{\quad}Q \end{bmatrix} \tag{39}$$

2) TRANSFORMATION MATRIX T_{B-A}

Suppose that a force F act on point A, the equivalent force at another point B will be:

$$\begin{cases} f_x^B = f_x^A \\ f_y^B = f_y^A \\ f_z^B = f_z^A \\ M_x^B = M_x^A - [\vec{BA}]_z \cdot f_y^A + [\vec{BA}]_y \cdot f_z^A \\ M_y^B = M_y^A + [\vec{BA}]_z \cdot f_x^A - [\vec{BA}]_x \cdot f_z^A \\ M_z^B = M_z^A - [\vec{BA}]_y \cdot f_x^A + [\vec{BA}]_x \cdot f_y^A \end{cases} \tag{40}$$

Formulate above equations group in matrix form, yield:

$$\begin{aligned} F^B &= \begin{bmatrix} I & 0 \\ P & I \end{bmatrix} \cdot F^A, \text{ with } P(\vec{BA}) \\ &= \begin{bmatrix} 0 & -[\vec{BA}]_z & [\vec{BA}]_y \\ [\vec{BA}]_z & 0 & -[\vec{BA}]_x \\ -[\vec{BA}]_y & [\vec{BA}]_x & 0 \end{bmatrix} \end{aligned} \tag{41}$$

Define the transformation matrix:

$$T_{B-A}(\vec{BA})=\begin{bmatrix} I & 0 \\ P & I \end{bmatrix} \tag{42}$$

C. DERIVATION OF THE COMPLIANCE-BASED MATRIX METHOD OF SERIAL AND PARALLEL MECHANISM

1) Transformed compliance matrix of a single flexure hinge

In the simplest case, namely the force vector and deformation vector are both in flexure hinge fixed local coordinate system $\{h\}$, and force are acting on the free end of the flexure hinge, the deformation can be calculated by:

$$\boldsymbol{D}_{\{h\}} = \boldsymbol{C}^h \cdot \boldsymbol{F}_{\{h\}} \tag{43}$$

However, in general case, force vector and deformation vector may be expressed in another coordinate system, or force may not act directly on the h point, but elsewhere in the mechanism, and then pass to the h point, etc. In order to make Eq. (11) more universal, three points matrix method [13] is introduced, with help of transformation matrix and rotation matrix:

$$\boldsymbol{D}_{b\{G\}} = \underbrace{[\boldsymbol{T}_{h-b}]^{\mathrm{T}} \left[\boldsymbol{R}_{\{h\}-\{G\}}\right]^T \underbrace{\boldsymbol{C}^h \left[\boldsymbol{R}_{\{h\}-\{G\}}\right] [\boldsymbol{T}_{h-a}] \boldsymbol{F}_{a\{G\}}}_{=\boldsymbol{D}_{h\{h\}}}}_{=\boldsymbol{D}h\{G\}} \tag{44}$$

For simplicity, define:

$$\boldsymbol{J}_{G-h} \otimes \boldsymbol{C}^h = [\boldsymbol{T}_{h-b}]^T \left[\boldsymbol{R}_{\{h\}-\{G\}}\right]^T \boldsymbol{C}^h \left[\boldsymbol{R}_{\{h\}-\{G\}}\right] [\boldsymbol{T}_{h-a}] \tag{45}$$

The so-called three points, namely point a - the point of application of force, point h - end point of the flexure hinge, and point b - interest point of deformation(displacement). The proof process is as follows:

1) Transfer the force to the flexure hinge and transform it into local coordinate, calculate the deformation of the flexure hinge $\boldsymbol{D}_{b\{G\}}$;
2) Transform the $\boldsymbol{D}_{b\{G\}}$ to the specified coordinate (e.g. global coordinate system) with $\boldsymbol{R}_{\{G\}-\{h\}}$, since rotation matrix is orthogonal matrix, the following formula always holds:

$$\boldsymbol{R}_{\{G\}-\{h\}} = [\boldsymbol{R}_{\{h\}-\{G\}}]^{-1} = [\boldsymbol{R}_{\{h\}-\{G\}}]^T \tag{46}$$

3) Now $\boldsymbol{D}_{h\{G\}}$ is known, based on small deformation assumption, $\boldsymbol{D}_{b\{G\}}$ can be further calculate by

$$\begin{cases} d_x^b = d_x^h + [\vec{hb}]_z \cdot \theta_y^h - [\vec{hb}]_y \cdot \theta_z^h \\ d_y^b = d_y^h - [\vec{hb}]_z \cdot \theta_x^h + [\vec{hb}]_x \cdot \theta_z^h \\ d_z^b = d_z^h + [\vec{hb}]_y \cdot \theta_x^h - [\vec{hb}]_x \cdot \theta_y^h \\ \theta_x^b = \theta_x^h \\ \theta_y^b = \theta_y^h \\ \theta_z^b = \theta_z^h \end{cases} \tag{47}$$

Rewrite above equations group into matrix form, yield:

$$\underbrace{\begin{bmatrix} d_x^b \\ d_y^b \\ d_z^b \\ \theta_x^b \\ \theta_y^b \\ \theta_z^b \end{bmatrix}}_{\boldsymbol{D}_{b\{G\}}} = \underbrace{\left[\begin{array}{ccc} & 0 & [\vec{hb}]_z & -[\vec{hb}]_y \\ I & -[\vec{hb}]_z & 0 & [\vec{hb}]_x \\ & [\vec{hb}]_y & -[\vec{hb}]_x & 0 \\ \hdashline 0 & & I & \end{array}\right]}_{\boldsymbol{T}_{b-h}} \underbrace{\begin{bmatrix} d_x^h \\ d_y^h \\ d_z^h \\ \theta_x^h \\ \theta_y^h \\ \theta_z^h \end{bmatrix}}_{\boldsymbol{D}_{h\{G\}}} \tag{48}$$

Compared to Eq. (42), it can be found that $\boldsymbol{T}_{b-h}$ is the transpose of T_{h-b}:

$$\boldsymbol{T}_{b-h} = [\boldsymbol{T}_{h-b}]^T \tag{49}$$

1) SERIAL MECHANISM

Assume there is a serial chain with one fixed end and one free end, comprises multi flexure hinges interconnected with several rigid links. The point load interacts and deforms with all the flexible hinges on the series chain between the point of force and the fixed end, so that the displacement at the point of interest p is calculated by the linear superposition of all the individual displacements generated by the interaction between the load and any flexible hinge. The individual displacement of a flexure hinge is derived by Eq. (12), the linear superposition can be formulated as:

$$\boldsymbol{D}_{\{G\}}^{chain} = \sum \boldsymbol{J}_{G-hi} \otimes \boldsymbol{C}^{hi} \cdot \boldsymbol{F}_{\{G\}} \tag{50}$$

2) PARALLEL MECHANISM

Since multi limbs parallelly connect at a center point O, the displacement for each limb is identical, namely $D^O = D^{limb1} = D^{limb2} = \ldots = D^{limbn}$. On the same time, the external force f acting on the point O is the sum of the reaction forces of each limb, namely:

$$\begin{aligned} f &= f^{limb1} + f^{limb2} + \cdots + f^{limbn} \\ &= \sum [C^{limbi}]^{-1} D^{limbi} \end{aligned} \tag{51}$$

The force-deformation relationship of the parallel mechanism is:

$$[C^{Parallel}]^{-1} \cdot D^O = f = \sum [C^{limbi}]^{-1} D^{limbi} \tag{52}$$

Hence,

$$C^{Parallel} = (\sum [C^{limbi}]^{-1})^{-1} \tag{53}$$

D. DERIVATION OF THE COMPLIANCE-BASED MATRIX OF 3-PRS CPM

Although in general, limb is defined as the parts between the moving platform and the base, each limb includes the flexible hinges at both ends and the rigid connecting rod in the middle. However, for ease of operation, the skeleton of the piezoelectric ceramic and the moving platform is considered as extended part of the limb. In order to avoid confusion, this limb including extended part is called "fictitious limb" in this paper.

It is worth noting that, the rigid bodies (rigid link between in the middle and the skeleton of the platform) in fictitious limb are not deformable, which equivalent to a flexure hinge whose compliance matrix's elements are all zero. On the contrary, since piezoelectric ceramic's deformation is freely controlled according to demand, it is regarded as a soft spring in moving direction. Based on these reasonable simplifications, the transformed compliance matrix of j^{th} fictitious limb is:

$$\begin{aligned} \mathbf{C}^{flimbj} &= \sum_{i=1}^{5} \mathbf{J}^j_{G-hi} \otimes \mathbf{C}^{hi} \\ &= \sum_{i=1}^{5} \left[\mathbf{T}^j_{hi-o}\right]^T \left[\mathbf{R}^j_{\{hi\}-\{G\}}\right]^T \mathbf{C}^{hi} \left[\mathbf{R}^j_{\{hi\}-\{G\}}\right] \left[\mathbf{T}^j_{hi-o}\right] \end{aligned} \tag{54}$$

where $\mathbf{C}^{h1}$ refer to the piezoelectric ceramic actuator, $\mathbf{C}^{h2}$ refer to the revolute flexure hinge, $\mathbf{C}^{h3}$ refer to the rigid link in between, $\mathbf{C}^{h4}$ refer to the spherical flexure hinge and $\mathbf{C}^{h5}$ refer to the skeleton of the platform. $\mathbf{C}^{h2}$ and $\mathbf{C}^{h4}$ can be obtained according to Appendix B1.1. $\mathbf{C}^{h1}$, $\mathbf{C}^{h3}$ and $\mathbf{C}^{h5}$ are set as follows:

$$\mathbf{C}^{h1} = \begin{bmatrix} 0\,0 & 0 & 0\,0\,0 \\ 0\,0 & 0 & 0\,0\,0 \\ 0\,0 & 100000 & 0\,0\,0 \\ 0\,0 & 0 & 0\,0\,0 \\ 0\,0 & 0 & 0\,0\,0 \\ 0\,0 & 0 & 0\,0\,0 \end{bmatrix}, \mathbf{C}^{h3} = \mathbf{C}^{h5}$$

$$= \begin{bmatrix} 0\,0\,0\,0\,0\,0 \\ 0\,0\,0\,0\,0\,0 \\ 0\,0\,0\,0\,0\,0 \\ 0\,0\,0\,0\,0\,0 \\ 0\,0\,0\,0\,0\,0 \\ 0\,0\,0\,0\,0\,0 \end{bmatrix} \tag{55}$$

Noted that, when $i = 5$, $\overrightarrow{hio}^j_{\{G\}}$ equal to zero vector. $\mathbf{R}^j_{\{hi\}-\{G\}} = \mathbf{R}_{\{hi\}-\{G\}}(0, \beta_i, \varphi_j)$ can be calculated by (7) with

$$\beta_i = \begin{cases} -\pi/2, & i = 1, 5 \\ -\pi/2 + \theta, & i = 2, 3, 4 \end{cases} \tag{56}$$

$\mathbf{T}^j_{hi-o} = \mathbf{T}^j_{hi-o}(\overrightarrow{hio}^j_{\{G\}})$ can be calculated by (42) when $\overrightarrow{hio}^j_{\{G\}}$ is given as follows:

$$\begin{aligned} \overrightarrow{hio}^j_{\{G\}} &= \overrightarrow{hih4}^j_{\{G\}} + \overrightarrow{h4h5}^j_{\{G\}} \\ &= L_i \cdot \left[-\cos\theta \cdot \cos\varphi_j \;\; -\cos\theta \cdot \sin\varphi_j \;\; \sin\theta \right] \\ &\quad + r_{top} \cdot \left[-\cos\varphi_j \;\; -\sin\varphi_j \;\; 0 \right] \end{aligned} \tag{57}$$

with

$$L_i = \begin{cases} l_{revolute} + l_{rigidlink} + l_{spherical}, & i = 1 \\ l_{rigidlink} + l_{spherical}, & i = 2 \\ l_{spherical}, & i = 3 \\ 0, & i = 4 \end{cases} \quad \text{and}$$

$$\varphi_j = \begin{cases} 0, & j = 1 \\ 2\pi/3, & j = 2 \\ -2\pi/3, & j = 3 \end{cases} \tag{58}$$

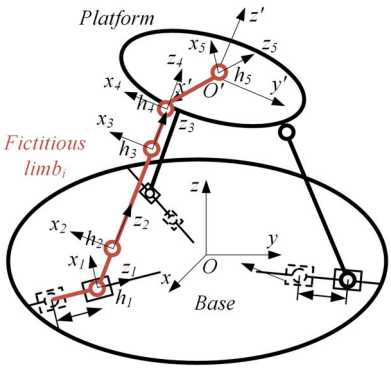

FIGURE 15. Coordinate systems on fictitious limb.

REFERENCES

[1] S. Yang, Q. Xu, and Z. Nan, "Design and development of a dual-axis force sensing MEMS microgripper," *J. Mech. Robot.*, vol. 9, no. 6, Dec. 2017, Art. no. 061011.

[2] Y. Tian, Y. Ma, F. Wang, K. Lu, and D. Zhang, "A novel XYZ micro/nano positioner with an amplifier based on L-shape levers and half-bridge structure," *Sens. Actuators A, Phys.*, vol. 302, Feb. 2020, Art. no. 111777.

[3] R. D. Dsouza, K. P. Navin, T. Theodoridis, and P. Sharma, "Design, fabrication and testing of a 2 DOF compliant flexural microgripper," *Microsyst. Technol.*, vol. 24, no. 9, pp. 3867–3883, Sep. 2018.

[4] F. Chen, W. Dong, M. Yang, L. Sun, and Z. Du, "A PZT actuated 6-DOF positioning system for space optics alignment," *IEEE/ASME Trans. Mechatronics*, vol. 24, no. 6, pp. 2827–2838, Dec. 2019.
[5] Z. Du, R. Shi, and W. Dong, "A piezo-actuated high-precision flexible parallel pointing mechanism: Conceptual design, development, and experiments," *IEEE Trans. Robot.*, vol. 30, no. 1, pp. 131–137, Feb. 2014.
[6] A. Ruiz, F. J. Campa, C. Roldán-Paraponiaris, O. Altuzarra, and C. Pinto, "Experimental validation of the kinematic design of 3-PRS compliant parallel mechanisms," *Mechatronics*, vol. 39, pp. 77–88, Nov. 2016.
[7] A. Ruiz, F. J. Campa, O. Altuzarra, S. Herrero, and M. Diez, "Mechatronic model of a compliant 3PRS parallel manipulator," *Robotics*, vol. 11, no. 1, p. 4, Dec. 2021.
[8] S. Xiao, Y. Li, and Q. Meng, "Mobility analysis of a 3-PUU flexure-based manipulator based on screw theory and compliance matrix method," *Int. J. Precis. Eng. Manuf.*, vol. 14, no. 8, pp. 1345–1353, Aug. 2013.
[9] W. Dan and F. Rui, "Design and nonlinear analysis of a 6-DOF compliant parallel manipulator with spatial beam flexure hinges," *Precis. Eng.*, vol. 45, pp. 365–373, Jul. 2016.
[10] M. Yang, Z. Du, F. Chen, W. Dong, and D. Zhang, "Kinetostatic modelling of a 3-PRR planar compliant parallel manipulator with flexure pivots," *Precis. Eng.*, vol. 48, pp. 323–330, Apr. 2017.
[11] F. Chen, Q. Zhang, Y. Gao, and W. Dong, "Design and analysis of a compact piezo-actuated microgripper with a large amplification ratio," *J. Mech. Des.*, vol. 144, no. 5, pp. 1–10, May 2022.
[12] N. Lobontiu and E. Garcia, "Analytical model of displacement amplification and stiffness optimization for a class of flexure-based compliant mechanisms," *Comput. Struct.*, vol. 81, no. 32, pp. 2797–2810, Dec. 2003.
[13] N. Lobontiu, "Compliance-based matrix method for modeling the quasi-static response of planar serial flexure-hinge mechanisms," *Precis. Eng.*, vol. 38, no. 3, pp. 639–650, Jul. 2014.
[14] S. Noveanu, N. Lobontiu, J. Lazaro, and D. Mandru, "Substructure compliance matrix model of planar branched flexure-hinge mechanisms: Design, testing and characterization of a gripper," *Mechanism Mach. Theory*, vol. 91, pp. 1–20, Sep. 2015.
[15] J. Li and G. Chen, "A general approach for generating kinetostatic models for planar flexure-based compliant mechanisms using matrix representation," *Mechanism Mach. Theory*, vol. 129, pp. 131–147, Nov. 2018.
[16] E. Rouhani and M. J. Nategh, "An elastokinematic solution to the inverse kinematics of microhexapod manipulator with flexure joints of varying rotation center," *Mechanism Mach. Theory*, vol. 97, pp. 127–140, Mar. 2016.
[17] H. Xu, H. Zhou, S. Tan, J.-A. Duan, and F. Hou, "A six-degree-of-freedom compliant parallel platform for optoelectronic packaging," *IEEE Trans. Ind. Electron.*, vol. 68, no. 11, pp. 11178–11187, Nov. 2021.
[18] H. Xu, H. Zhou, S. Tan, Z. Kong, and J.-A. Duan, "A 3-prismatic-revolute-spherical compliant parallel platform for optoelectronic packaging," *J. Mech. Sci. Technol.*, vol. 36, no. 6, pp. 2685–2694, Jun. 2022.
[19] F. Hou, M. Luo, and Z. Zhang, "An inverse kinematic analysis modeling on a 6-PSS compliant parallel platform for optoelectronic packaging," *CES Trans. Electr. Mach. Syst.*, vol. 3, no. 1, pp. 81–87, Mar. 2019.
[20] Y. Tian, B. Shirinzadeh, and D. Zhang, "Closed-form compliance equations of filleted V-shaped flexure hinges for compliant mechanism design," *Precis. Eng.*, vol. 34, no. 3, pp. 408–418, Jul. 2010.
[21] J. R. Hutchinson, "Shear coefficients for Timoshenko beam theory," *J. Appl. Mech.*, vol. 68, no. 1, pp. 87–92, Jan. 2001.
[22] G. Chen, X. Shao, and X. Huang, "A new generalized model for elliptical arc flexure hinges," *Rev. Sci. Instrum.*, vol. 79, no. 9, pp. 1–10, 2008.

JUNJIE WEI was born in Foshan, Guangdong, in 1993. He received the B.S. degree in mechanical and electronic engineering from Chongqing University, in 2016, and the M.S. degree in mechatronics and information engineering from the Karlsruhe Institute of Technology, in 2020.

He is currently with the Jihua Laboratory and participating in the design and simulation of parallel robot. His research interests include machine vision and robot motion and control.

HAI BI received the B.E. and M.E. degrees in chemistry from Jilin University, in 2007 and 2010, respectively, and the Ph.D. degree in physics from the Technical University of Munich, in 2014.

He was working with Harvard University, SEAS, from 2015 to 2019. He moved to the Jihua Laboratory, as a Principle Investigator, in 2020, and he Founded the Germany–China Joint Innovation Laboratory. His research interests include the super-resolution microscopy with near-field enhanced mechanism, optoelectronic devices of organic semiconductors, and organic semiconductor.

HONG YAO received the B.S. degree in naval architecture and marine engineering and the M.S. degree in design and construction of naval architecture and ocean structure from the Dalian University of Technology, Dalian, China, in 2017 and 2020, respectively. Since 2020, he has been a Junior Engineer with the Jihua Laboratory, Foshan, China. His current research interests include the design and control of piezoelectric actuator in precision positioning.

FANGXIN CHEN (Member, IEEE) was born in Chengdu, Sichuan, China, in 1992. He received the B.S. degree in mechanical engineering from Jilin University, Changchun, China, in 2015, and the Ph.D. degree in mechatronics from the Harbin Institute of Technology, Harbin, China, in 2020.

Since 2020, he has been a Research Assistant with the Jihua Laboratory, Foshan, China. He is the author of more than 20 articles and more than ten inventions. His research interests include the development of the compliant mechanism, the fundamental study of flexure hinges, the structure synthesis of parallel robots, and the development of micromanipulation robot.